

Effects of stratospheric aerosols and thin cirrus clouds on the atmospheric correction of ocean color imagery: simulations

Howard R. Gordon, Tianming Zhang, Fan He, and Kuiyuan Ding

Using simulations, we determine the influence of stratospheric aerosol and thin cirrus clouds on the performance of the proposed atmospheric correction algorithm for the moderate resolution imaging spectroradiometer (MODIS) data over the oceans. Further, we investigate the possibility of using the radiance exiting the top of the atmosphere in the 1.38- μm water vapor absorption band to remove their effects prior to application of the algorithm. The computations suggest that for moderate optical thicknesses in the stratosphere, i.e., $\tau_s \leq 0.15$, the stratospheric aerosol-cirrus cloud contamination does not seriously degrade the MODIS except for the combination of large ($\sim 60^\circ$) solar zenith angles and large ($\sim 45^\circ$) viewing angles, for which multiple-scattering effects can be expected to be particularly severe. The performance of a hierarchy of stratospheric aerosol/cirrus cloud removal procedures for employing the 1.38- μm water vapor absorption band to correct for stratospheric aerosol/cirrus clouds, ranging from simply subtracting the reflectance at 1.38 μm from that in the visible bands, to assuming that their optical properties are known and carrying out multiple-scattering computations of their effect by the use of the 1.38- μm reflectance-derived concentration, are studied for stratospheric aerosol optical thicknesses at 865 nm as large as 0.15 and for cirrus cloud optical thicknesses at 865 nm as large as 1.0. Typically, those procedures requiring the most knowledge concerning the aerosol optical properties (and also the most complex) performed the best; however, for $\tau_s \leq 0.15$, their performance is usually not significantly better than that found by applying the simplest correction procedure. A semiempirical algorithm is presented that permits accurate correction for thin cirrus clouds with τ_s as large as unity when an accurate estimate of the cirrus cloud scattering phase function is provided, and as large as 0.5 when a coarse approximation to the phase function is used. Given estimates of the stratospheric aerosol optical properties, the implementation of the algorithm by using a set of lookup tables appears to be straightforward. © 1997 Optical Society of America

1. Introduction

The radiance exiting the ocean-atmosphere system contains information on the concentration of marine phytoplankton—the first link in the marine food chain—through the variations it produces in the color of the water.¹ The flight of the Coastal Zone Color Scanner (CZCS)^{2,3} was a proof-of-concept mission to demonstrate the feasibility of quantitatively estimating the concentration of chlorophyll *a*, a photosynthetic pigment contained in phytoplankton and used as a surrogate for its concentration. Based on the

success of the CZCS, a number of instruments for ocean color measurements will be launched in the 1990's, e.g., the sea-viewing wide field-of-view sensor (SeaWiFS)⁴ and the moderate resolution imaging spectroradiometer (MODIS).⁵

The contribution from beneath the sea surface to the radiance exiting the ocean-atmosphere system in the visible is very small, i.e., at most 10–20% of the total in the blue and less at longer wavelengths. The remainder of the radiance is due to scattering from the atmosphere and reflection from the sea surface. Thus, it is of the utmost importance to remove these interfering effects in order to isolate the water-leaving radiance that contains the information regarding phytoplankton. This process is termed atmospheric correction. The CZCS atmospheric correction algorithm,⁶ which was based on the single-scattering approximation, was not sufficiently accurate to be applied to the SeaWiFS and the MO-

The authors are with the Department of Physics, University of Miami, Coral Gables, Florida 33124.

Received 4 March 1996; revised manuscript received 15 July 1996.

0003-6935/97/030682-16\$10.00/0

© 1997 Optical Society of America

DIS because they have far better radiometric sensitivity. Gordon and Wang⁷ developed a multiple-scattering correction algorithm suitable for use with these sensors. The algorithm assumes that all of the aerosol in the atmosphere is in the marine boundary layer (MBL) and uses aerosol models to deal with the multiple scattering. The requirement for aerosol models stems from the fact that the magnitude of the multiple-scattering effects is model dependent.

In some situations, e.g., following volcanic eruptions or when there are thin cirrus clouds present, there can be significant quantities of aerosol in the stratosphere. Although Gordon and Castaño⁸ showed that the presence of the El Chichón aerosol⁹ had little effect on the CZCS atmospheric correction, at the higher correction accuracy required for the SeaWiFS and the MODIS the Gordon and Wang⁷ algorithm may be degraded by the presence of stratospheric aerosol. In the case of the SeaWiFS, influence of the stratospheric aerosol on the absorption by the O₂ A band at 762 nm introduces an additional complication. This has been discussed in detail by Ding and Gordon,¹⁰ and as there is no direct way of assessing the presence of stratospheric aerosol with the SeaWiFS, we do not discuss that sensor further here. In contrast, the MODIS, which avoids the O₂ A band, is equipped with a spectral band at 1.38 μm that can be used to assess the contamination by stratospheric aerosol. This spectral band is centered on a strong water vapor absorption band, and photons penetrating through the stratosphere will usually be absorbed by water vapor in the free troposphere.¹¹ Thus, any radiance measured at 1.38 μm can, in the first approximation, be assumed to be scattered by the stratospheric aerosol alone. This provides a mechanism for estimating the stratospheric contribution. In this paper we assess the degradation in atmospheric correction of the MODIS resulting from the presence of stratospheric aerosols. We assume that the radiance measured at 1.38 μm is totally due to the stratosphere and examine several possibilities for using this information in the proposed atmospheric correction algorithm⁷ to correct ocean color imagery.

2. Proposed SeaWiFS–MODIS Atmospheric Correction Algorithm

The Gordon and Wang⁷ atmospheric correction algorithm uses the reflectance, ρ , rather than the radiance, L . These are related by $\rho = \pi L / F_0 \cos \theta_0$, where F_0 is the extraterrestrial solar irradiance and θ_0 is the solar zenith angle. In the absence of stratospheric aerosol, the total reflectance of the ocean-atmosphere system, $\rho_t(\lambda)$, measured at a wavelength, λ , can be decomposed as follows:

$$\rho_t(\lambda) = \rho_r(\lambda) + \rho_a(\lambda) + \rho_{ra}(\lambda) + t(\theta_v, \lambda)\rho_w(\lambda),$$

where $\rho_r(\lambda)$ is the reflectance resulting from multiple scattering by air molecules (Rayleigh scattering) in the absence of aerosols, $\rho_a(\lambda)$ is the reflectance resulting from multiple scattering by aerosols in the ab-

sence of the air, $\rho_{ra}(\lambda)$ is the interaction term between molecular and aerosol scattering,¹² and ρ_w is the desired water-leaving reflectance. In this equation, t is the diffuse transmittance of the atmosphere¹³ along the viewing direction specified by θ_v , the angle between the normal to the sea surface and the sensor. Radiance arising from specular reflection of direct sunlight from the sea surface (Sun glitter) has been ignored. This means that the correction cannot be valid near the glitter pattern. The influence of whitecaps has also been ignored under the assumption that their contribution can be removed, prior to application of the correction algorithm, by using an estimate of the surface wind speed.¹⁴

The goal of the atmospheric correction is the retrieval of ρ_w from ρ_t . This is effected by measuring ρ_t in the near-infrared (NIR) near 765 and 865 nm for the SeaWiFS and near 750 and 865 nm for the MODIS. In this spectral region, ρ_w can be taken to be zero because of the strong absorption by the water itself; ρ_r can be computed given an estimate of the atmospheric pressure, so $\rho_a + \rho_{ra}$ can be determined directly in the NIR. From a set of candidate aerosol models, the spectral variation of $\rho_a + \rho_{ra}$ in the NIR is used to select a pair of aerosol models for accounting for multiple scattering and for determining the spectral dependence of $\rho_a + \rho_{ra}$ for extrapolation into the visible, thus providing ρ_w there.⁷ In the absence of stratospheric aerosol, simulations suggest that this algorithm will meet the goal of retrieval of ρ_w at 443 nm with an error ≤ 0.001 – 0.002 , i.e., an error of $\leq 5\%$ in ρ_w in the blue in very clear ocean water.

Incorporation of multiple scattering is effected through the use of lookup tables based on a large number ($\sim 33,000$) of radiative transfer simulations that use various aerosol models¹⁵ thought to be representative of aerosols occurring over the oceans. In the simulations it was assumed that all of the aerosol is resident in the MBL, i.e., the simulations were carried out by using an accurate (error $\leq 0.1\%$) two-layer radiative transfer code, with aerosols occupying the lower layer and molecular (Rayleigh) scattering occupying the upper layer. This vertical structure is similar to that normally found over the oceans, i.e., typically most of the aerosol is in the MBL.¹⁶

3. Simulation of the Effects of Stratospheric Aerosol

In situations in which there is significant stratospheric aerosol present, the aerosol vertical profile described in Section 2 is very unrealistic. A more realistic profile would be a three-layer atmosphere with aerosol in both the lower and upper layers and molecular scattering in the central layer. This is the profile that we adopt for simulating ρ_t in the presence of stratospheric aerosol.

We examine four different stratospheric aerosol models. The first is the background stratospheric aerosol¹⁷ consisting of a 75% solution of H₂SO₄ with

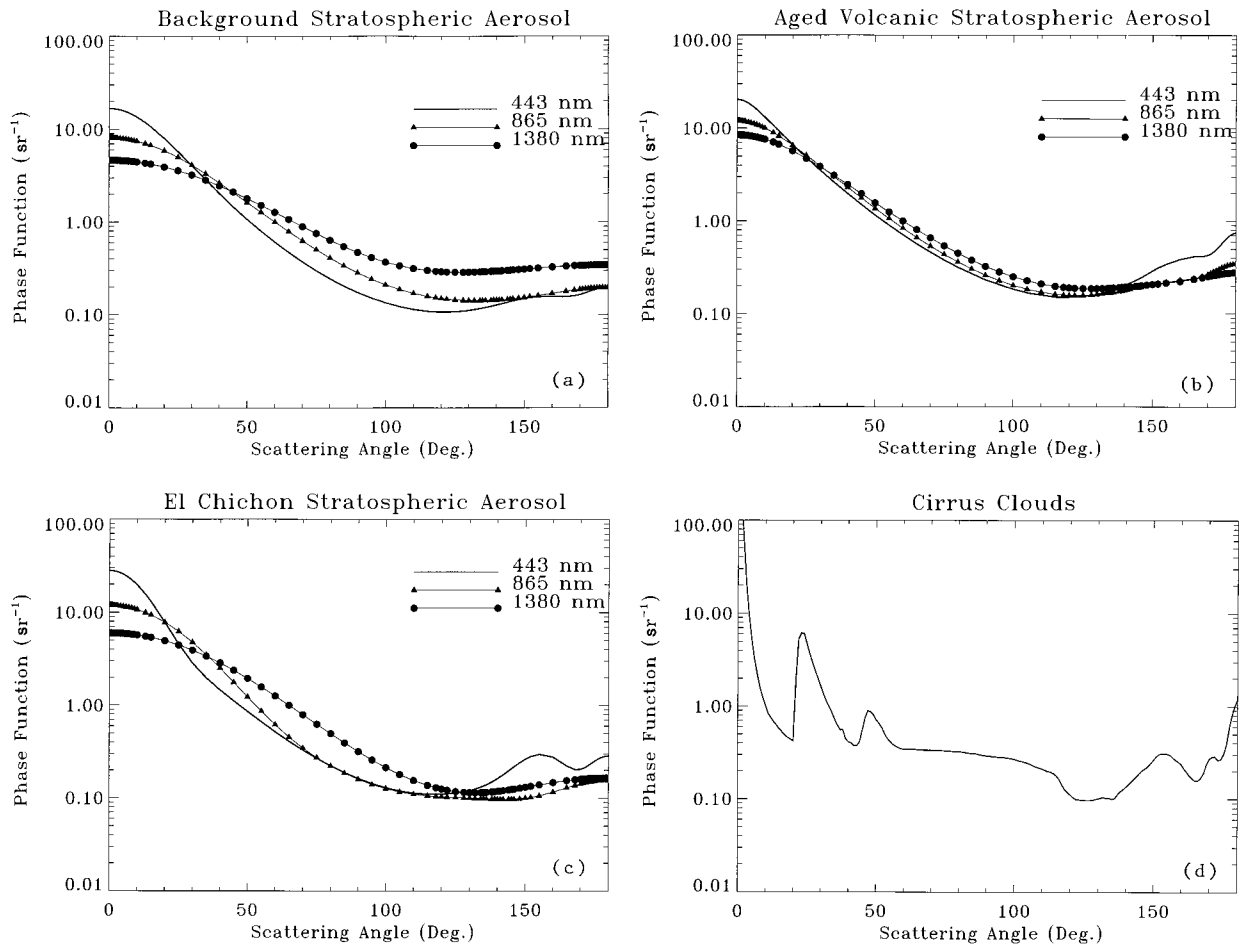


Fig. 1. Phase functions for the various stratospheric aerosol models used in the study: (a) background, (b) aged volcanic ash, (c) El Chichón, (d) thin cirrus clouds.

a size distribution given by

$$\frac{dn}{dD} = 81D \exp(-9D),$$

where dn is the number of particles per unit volume with diameters (D) in micrometers between D and $D + dD$. The second is the El Chichón aerosol,⁹ also a 75% solution of H_2SO_4 , with a size distribution of

$$\frac{dn}{dD} = 1.79386 \times 10^8 D^{12.65} \exp(-19.65D).$$

The third represents aged volcanic ash. It consists of an absorbing mineral distributed in size according to

$$\frac{dn}{dD} = 1365.33D \exp(-11.3137\sqrt{D}),$$

with a wavelength-independent index of refraction of $m = 1.50 - 0.008i$. For the background and the El Chichón aerosol, the index of refraction is taken from Palmer and Williams.¹⁸ The final aerosol model is that for thin cirrus clouds taken from Takano and Liou.¹⁹ In this case we assume that the scattering

properties of the thin cirrus clouds are independent of wavelength. The scattering phase functions for these four models are presented in Figs. 1(a)–1(d), and the spectral variation in their extinction (or stratospheric optical thickness, τ_s) is presented in Fig. 2. The first

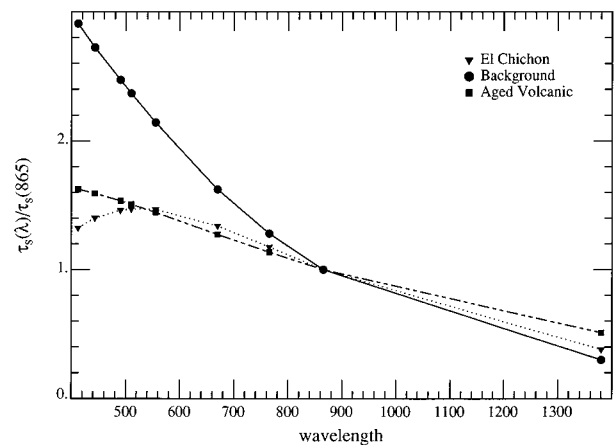


Fig. 2. Spectral variation of τ_s for the various stratospheric aerosol models. The cirrus cloud model is omitted because $\tau_s(\lambda)$ is constant.

three were calculated from the size distributions and the refractive indices by using Mie theory. The fourth was taken from the tabulated values of Ref. 19. Note the significant spectral variation of the shape of some of the aerosol phase functions.

As suggested above, we simulated the reflectance in the presence of stratospheric aerosol by using a three-layer radiative transfer code. The lower layer contained the Shettle and Fenn¹⁵ maritime aerosol at 80% relative humidity (M80). This was used as the MBL aerosol because, in the absence of stratospheric aerosol, the performance of the atmospheric correction algorithm is excellent (the error in ρ_w found by Gordon and Wang⁷ was less than ~ 0.0005 for this aerosol) and thus provides an ideal choice for an examination of the interfering effects of the stratospheric aerosol. The upper layer contains the stratospheric aerosol and the middle layer exhibits only molecular scattering. A Fresnel-reflecting flat sea surface constitutes the lower boundary. There is no radiance exiting the ocean, i.e., all photons penetrating the sea surface are absorbed. In the case of the MODIS, for the reflectance at 1380 nm to be simulated, a one-layer model with a totally absorbing lower boundary (no Fresnel reflection) was employed. The rationale for this is the assumption that all radiation penetrating through the stratosphere at this wavelength is absorbed by water vapor in the troposphere, so no radiance is reflected to the top of the atmosphere from below the stratospheric layer. Note that for the purpose of utilizing the 1380-nm MODIS band to correct for the stratospheric aerosol, this is the ideal setting, i.e., all of the reflected radiance at 1380 nm is due to the stratosphere, and there is no contamination from Rayleigh scattering in the free troposphere (middle layer), aerosol scattering in the MBL (lower layer), or reflection from the sea surface.

4. Impact of Stratospheric Aerosol on Atmospheric Correction

As described above, we simulated $\rho_t^{(s)}$ at 443, 765, 865, and 1380 nm by using a three-layer model of the atmosphere. The upper layer used the four stratospheric aerosol models with a stratospheric optical thickness of $\tau_s = 0.05$ and 0.15 at 865 nm. A maritime aerosol (M80) with a MBL optical thickness of $\tau_b = 0.15$ and 0.30 was placed in the lowest layer. There was no aerosol (only Rayleigh scattering) in the middle layer. Seven geometries were simulated: near-nadir viewing ($\theta_v \approx 0$) and viewing near the scan edge ($\theta_v \approx 45^\circ$) in the perpendicular plane, both for solar zenith angles of $0, 20^\circ, 40^\circ,$ and 60° . $\theta_0 = 0$ and $\theta_v \approx 0$ were not examined because they would be at the center of the Sun's glitter pattern. For the background, aged volcanic ash, and El Chichón aerosols, the computations were performed by using a successive-order-of-scattering radiative transfer code.²⁰ In the case of the cirrus cloud model, a Monte Carlo code was used because the presence of considerable angular structure in the scattering phase function (Fig. 1) would have required computation of too many Fourier coefficients in the azimuthal decomposition of the radiance in the

successive-order-of-scattering code to provide a reliable simulation.

The simulated values of $\rho_t^{(s)}$ at 443, 765, and 865 were then inserted into the Gordon and Wang⁷ atmospheric correction algorithm to retrieve $t\rho_w(\lambda)$, the water-leaving radiance transmitted to the top of the atmosphere. The reflectance at 1380 nm was not used and the presence of the stratospheric aerosol was simply ignored. The results of these simulations are presented in Fig. 3 for the various combinations of τ_s , τ_b , and the stratospheric aerosol model. In this figure we present histograms of the error for each stratospheric model. The taller bars in Fig. 3 represent the *maximum* value of $|\Delta[t\rho_w(\lambda)]|$ for $\lambda = 443$ nm for the seven combinations of angles. Typically, this occurs at the scan edge with $\theta_0 = 60^\circ$, i.e., at the position where multiple scattering is expected to be most severe. The shorter bars in the figure represent the average of $|\Delta[t\rho_w(\lambda)]|$ for $\lambda = 443$ nm over the *remaining* six combinations of angles. The horizontal dashed line is the upper limit of the acceptable error, i.e., 0.002 . Figure 3 clearly shows that, even at small values of τ_s , stratospheric aerosols can degrade the performance of the atmospheric correction algorithm, particularly in geometries in which multiple scattering is expected to be large.

These results are based on simulations that assume τ_s at 865 to be either 0.05 or 0.15 for all of the stratospheric aerosol models. Is this a realistic range? For background conditions in the stratosphere, the optical thickness at 1000 nm from the Stratospheric Aerosol and Gas Experiment solar occultation data is typically ≤ 0.01 , while following a major volcanic eruption and subsequent global dispersal of the aerosol, e.g., El Chichón or Pinatubo, $\tau_s \sim 0.10$ at ~ 1000 nm (L. Thomason, NASA Langley Research Center, personal communication). Thus, in the case of the background aerosol model, τ_s at 865 nm is too high by at least a factor of 5, and one would expect the error shown in Fig. 3 to be much too large. Because of its low τ_s , the error that is due to the background stratospheric aerosol will be negligible, and we do not consider it further. In contrast, the values of τ_s used for the El Chichón and aged volcanic ash models are in the appropriate range, and Fig. 3 should be representative of the performance of the algorithm⁷ in the presence of aerosols with these properties. Clearly the aged volcanic ash causes the greater degradation in atmospheric correction, presumably because of its higher absorption. It should also be noted that the optical thickness (τ_b) in the MBL at 865 nm rarely exceeds 0.2 in the absence of aerosol transported from deserts or anthropogenic aerosol sources.²¹ Therefore, of the situations presented here, the most likely are those with $\tau_b(865) = 0.15$, i.e., Figs. 3(a) and 3(b). With these observations in mind, we conclude that typically the error in atmospheric correction caused by volcanically produced sulfate stratospheric aerosol should be ~ 0.002 , except near the scan edge at high solar zenith angles, whereas for aged volcanic ash the error is expected to be significantly larger at the same τ_s . Thus, if no

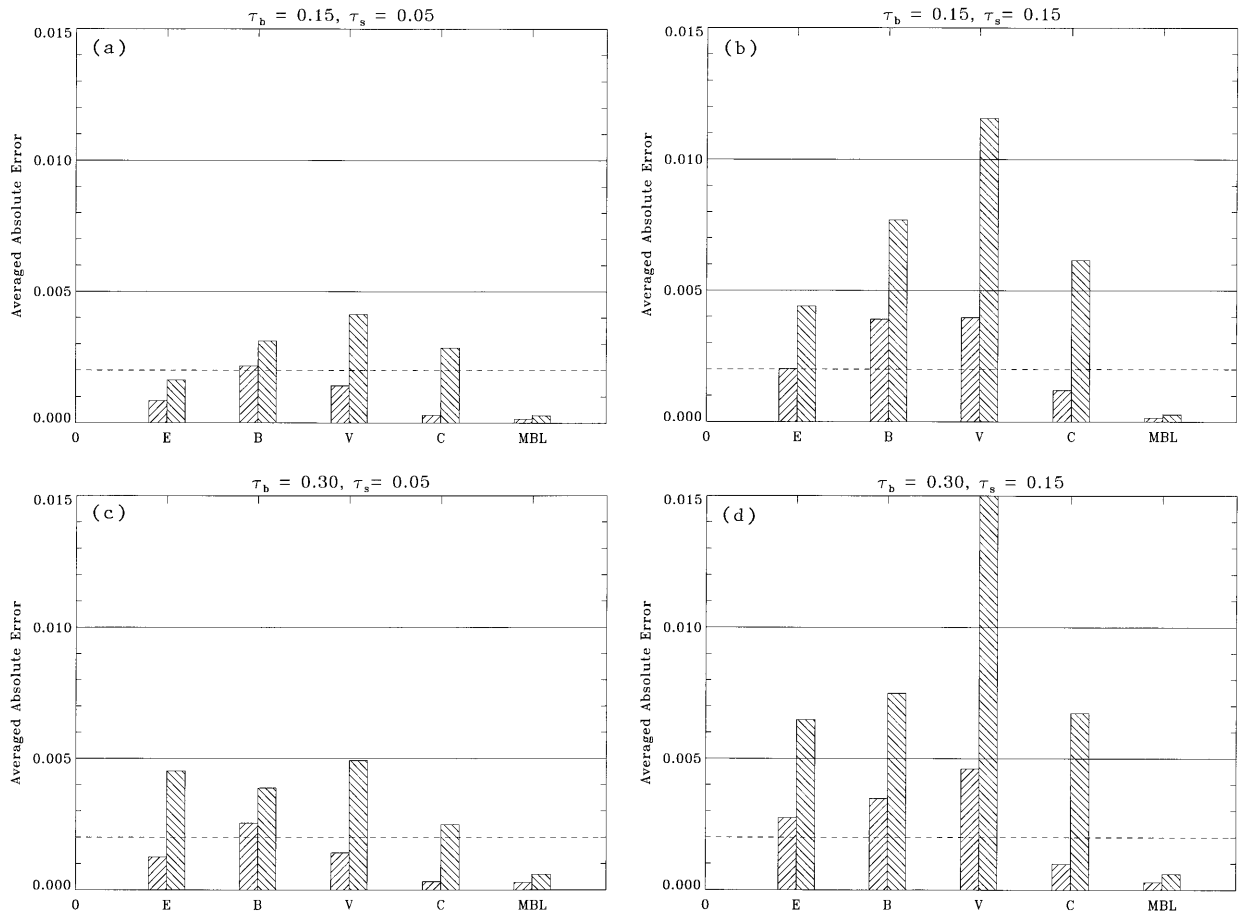


Fig. 3. Histogram of the average $|\Delta t_{\rho_{\omega}}(443)|$ (short bars) and the maximum $|\Delta t_{\rho_{\omega}}(443)|$ (tall bars) for all of the stratospheric aerosol models examined: (a) $\tau_b(865) = 0.15, \tau_s(865) = 0.05$; (b) $\tau_b(865) = 0.15, \tau_s(865) = 0.15$; (c) $\tau_b(865) = 0.30, \tau_s(865) = 0.05$; (d) $\tau_b(865) = 0.30, \tau_s(865) = 0.15$. E, B, V, C, and MBL refer to El Chichon, background, aged volcanic ash, cirrus clouds, and no stratospheric aerosol, respectively.

correction were made for the presence of stratospheric aerosol, in the case of aged volcanic ash one would have to wait for some of the ash to be removed from the atmosphere before an adequate atmospheric correction could be made. The observation that simply ignoring the stratospheric aerosol provides a reasonable correction for small τ_s agrees with the conclusion of Gordon and Castaño⁸ that the presence of the El Chichón aerosol had little effect on the CZCS atmospheric correction, taking into consideration that the CZCS did not require as accurate a correction.

In the case of cirrus clouds, we do not know the appropriate range of τ_s . Thus we carried out additional simulations for $\tau_s = 0.5$ and 1.0 . The results for all the cirrus cloud simulations are presented in Fig. 4. They show a consistent pattern of increasing error as τ_s increases, with the average error in atmospheric correction exceeding the goal (± 0.002) for τ_s between 0.15 and 0.50 .

5. Requirements for Precise Correction for Stratospheric Aerosols

Before discussing our efforts to remove the effects of stratospheric aerosols by using the 1380 nm band, we

find it useful to determine what would be required for a precise correction for stratospheric aerosols.

The most direct way of understanding the effects of adding stratospheric aerosol is to consider the adding or matrix operator method of solution of the radiative transfer equation. We first Fourier analyze the radiance field in the azimuthal direction, i.e.,

$$L(\tau, \theta_v, \phi_v) = L^{(0)}(\tau, \theta_v) + 2 \sum_{m=1}^{\infty} L^{(m)}(\tau, \theta_v) \cos m\phi_v,$$

where ϕ_v is the azimuth of propagation relative to the solar azimuth and θ_v is the angle between the propagation direction and the vertical. Then we assume that the radiance has been discretized into n upward and n downward streams, e.g., at the Gaussian quadrature values of angle θ_v . Finally, following Plass *et al.*,²² we write a particular Fourier component of the downward radiance as a column vector,

$$L^+(\tau) = \begin{bmatrix} L^+(\tau, \theta_1) \\ L^+(\tau, \theta_2) \\ \vdots \\ L^+(\tau, \theta_n) \end{bmatrix},$$

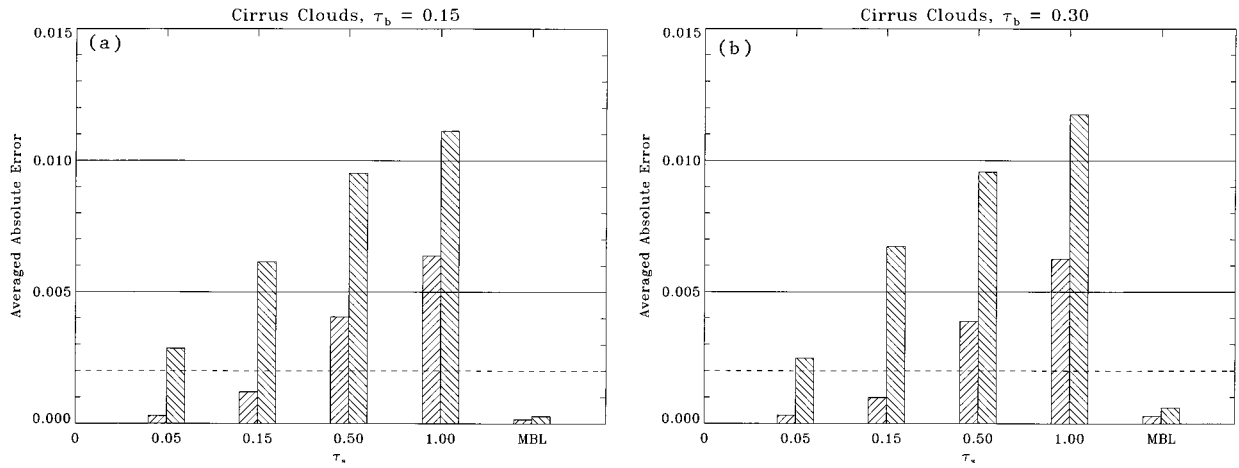


Fig. 4. Histogram of the average $|\Delta t \rho_w(443)|$ (short bars) and the maximum $|\Delta t \rho_w(443)|$ (tall bars) for the cirrus clouds for various combinations of τ_b and τ_s : (a) $\tau_b(865) = 0.15$, (b) $\tau_b(865) = 0.30$.

where θ_i are the polar angles for radiance in the downward direction and τ is the optical depth. Similarly, column vector $L^-(\tau)$ is composed of radiance propagating in the upward direction. Note that all of the equations that follow in this section refer to a single Fourier component, $L^{(m)}(\tau)$, and all of the quantities in the equations should carry the superscript, (m) ; however, to simplify the notation we suppress this superscript.

Consider a layer from τ_0 to τ_1 , and let $S^\pm(\tau_1, \tau_0)$ represent the exiting boundary radiances at $\tau_0(-)$ and $\tau_1(+)$ that are due to sources between τ_0 and τ_1 , e.g., the unscattered solar beam. Then the boundary radiances exiting the layer, $L^+(\tau_1)$ and $L^-(\tau_0)$, can be written in terms of the entering boundary radiances, $L^+(\tau_0)$ and $L^-(\tau_1)$, according to

$$\begin{aligned} L_1^+ &= t_{01}L_0^+ + r_{10}L_1^- + S_{01}^+, \\ L_0^- &= r_{01}L_0^+ + t_{10}L_1^- + S_{01}^-, \end{aligned}$$

where $L_1^+ \equiv L^+(\tau_1)$, and so on. The $n \times n$ matrices, r_{10} , r_{01} , t_{10} , and t_{01} , describe the transmittance and reflectance of any radiance that is incident upon the layer. If the layer is homogeneous, $r_{10} = r_{01}$ and $t_{10} = t_{01}$. If we write similar equations for a layer from τ_1 to τ_2 , and for the combined layer from τ_0 to τ_2 , we find that the r 's, t 's, and S 's for the combined layers can be determined from those of the individual layers.

In the problem of interest here, we take τ_0 to τ_1 to represent the stratospheric layer, and τ_1 to τ_2 to represent everything else, i.e., the troposphere, sea surface, and the body of the ocean. Consider the stratosphere alone. If the only source is the solar beam, which produces S_{01}^- , then the radiance exiting the top of the atmosphere (TOA) is just $L_0^- = S_{01}^-$. Now consider the second layer alone. Again, if the solar beam is the only source, $L_1^- = S_{12}^-$. In order to operate the Gordon and Wang⁷ algorithm, we require S_{12}^- , the radiance that the atmosphere-ocean system would have reflected were the stratosphere absent.

Combining the two layers and using the adding algorithm,²² we find

$$S_{02}^- = S_{01}^- + t_{10}(E - r_{12}r_{10})^{-1}(S_{12}^- + r_{12}S_{01}^+),$$

where E is the identity matrix. This can be solved for S_{12}^- , yielding

$$S_{12}^- = (E - r_{12}r_{10})t_{10}^{-1}(S_{02}^- - S_{01}^-) - r_{12}S_{01}^+.$$

However, because the stratospheric layer is in place, the solar beam illuminating the second layer must be reduced by a factor of $\exp[-(\tau_1 - \tau_0)/\mu_0]$, where $\mu_0 = \cos \theta_0$, so S_{12}^- in these equations must be replaced by $S_{12}^- \exp[-(\tau_1 - \tau_0)/\mu_0]$. Thus, the desired radiance is

$$\begin{aligned} S_{12}^- &= \exp(+\tau_s/\mu_0)[(E - r_{12}r_{10})t_{10}^{-1} \\ &\quad \times (S_{02}^- - S_{01}^-) - r_{12}S_{01}^+], \end{aligned} \quad (1)$$

where τ_s is the stratospheric optical thickness. Note that all of the quantities in this equation are functions of wavelength λ , and all quantities except τ_s refer to the m th Fourier component. The desired reflectance in the viewing direction, specified by (θ_v, ϕ_v) , is just $\rho_t = \pi S_{12}^-(\tau_1, \theta_v, \phi_v)/\mu_0 F_0$, where

$$\begin{aligned} S_{12}^-(\tau_1, \theta_v, \phi_v) &= S_{12}^{-(0)}(\tau_1, \theta_v) \\ &\quad + 2 \sum_{m=1}^{\infty} S_{12}^{-(m)}(\tau_1, \theta_v) \cos m\phi_v, \end{aligned}$$

and $\tau_1 = \tau_s$. Note that this requires only a single row of the matrices $(E - r_{12}r_{10})t_{10}^{-1}$ and r_{12} .

This equation delineates the quantities needed to retrieve $\rho_t(\lambda)$ from the TOA reflectance in the presence of stratospheric aerosol. Can we have enough information to retrieve ρ_t ? The measurement of the TOA radiance in the visible and NIR provides quantity S_{02}^- at any wavelength λ , but only in the viewing direction. As it is assumed that the TOA radiance at 1380 nm is due entirely to the stratosphere, its measurement would provide S_{01}^- at 1380 nm, but again only in the viewing direction. If we had a model of

the stratospheric aerosol, S_{01}^- at 1380 nm in the viewing direction could be used to estimate τ_s at 1380 nm. Then τ_s at 1380 nm and the aerosol model could be used to determine full matrices S_{01}^- , S_{01}^+ , r_{10} , and t_{10} at any wavelength.

Unfortunately, even with full knowledge of the optics of the stratosphere, neither operator r_{12} , the radiance reflectance matrix for the troposphere, sea surface, and ocean, nor full column vector S_{02}^- can be determined with precision as they depend on the (unknown) tropospheric aerosol properties and the (unknown) concentration, as well as the properties of the ocean. One could use standard models to estimate r_{12} to within a multiplicative constant; however, this constant would depend on the tropospheric aerosol concentration. Thus it appears impossible to estimate r_{12} . If this is set to zero, single- and multiple-reflection interactions between the stratosphere and troposphere are neglected.

6. Simplified Procedures for Correcting for Stratospheric Aerosol

As it is clear that a precise value of ρ_t cannot be derived based on the available information, we now examine several simplified procedures for correction for the presence of stratospheric aerosol. In the limit that $\tau_s \rightarrow 0$, we expect

$$T\rho_t = \rho_t^{(s)} - \delta\rho_t^{(s)}, \quad (2)$$

where $\rho_t^{(s)}$ is the reflectance of the entire ocean-atmosphere system in the presence of stratospheric aerosol, T is a transmittance factor that indicates the reduction in ρ_t that is due to the presence of the layer, and $\delta\rho_t^{(s)}$ is the reflectance added by the layer. As we expect the stratospheric perturbation to be small,⁸ our strategy for the MODIS is to try to estimate $\delta\rho_t^{(s)}$ and remove it from $\rho_t^{(s)}$ for an estimate of $T\rho_t$. T would then be estimated, and the existing atmospheric correction algorithm⁷ would be operated with the resulting ρ_t as the ocean-atmosphere reflectance. In this manner the existing algorithm would be used in the setting for which it was developed: a two-layer atmosphere (the effects of the third layer having been removed), with all of the aerosol in the lower layer. Thus the goal is to be able to remove as much of $\delta\rho_t^{(s)}$ from $\rho_t^{(s)}$ as possible.

Using the $\rho_t^{(s)}(\lambda)$ pseudodata described in Section 4, we examined atmospheric correction for the MODIS. We considered six possibilities for utilizing the 1380-nm band for correction for stratospheric aerosols. As we described in Section 3, we assumed that the reflectance at 1380 nm was totally due to the stratospheric aerosol. The six correction schemes for the removal of the stratospheric aerosol component follow.

1. The measured reflectances at 443, 765, and 865 nm were used in the Gordon and Wang algorithm as usual, i.e., no attention was paid to the fact that a stratospheric aerosol may be present [$\rho_t^{(s)}(\lambda)$ was assumed to be $\rho_t(\lambda)$], and the error in the atmospheric

correction at 443 nm was determined. This is identical to the procedure used to generate the results provided in Figs. 3 and 4.

2. The presence of stratospheric aerosol was incorporated into the algorithm simply by subtracting the reflectance at 1380 nm from that at 443, 765, and 865 nm, i.e., $T(\lambda)\rho_t(\lambda) = \rho_t^{(s)}(\lambda) - \rho_t^{(s)}(1380)$. The values of $\rho_t(\lambda)$ were then inserted into the correction algorithm, and the error in the correction at 443 nm was determined.

3. It was assumed that the spectral variation of the optical thickness of the stratospheric aerosol is known, e.g., from measurements from the surface. The reflectance at 1380 nm (which is entirely due to the stratospheric aerosol) was scaled by the ratio of the stratospheric optical depth at the given λ , $\tau_s(\lambda)$, to that at (or in the case of surface measurements, near) 1380 nm, and it was subtracted from the measured reflectances at the other wavelengths, i.e.,

$$T(\lambda)\rho_t(\lambda) = \rho_t^{(s)}(\lambda) - \frac{\tau_s(\lambda)}{\tau_s(1380)} \rho_t^{(s)}(1380).$$

The values of $\rho_t(\lambda)$ were then inserted into the correction algorithm and the error in the correction at 443 nm was determined.

4. It was assumed that accurate measurements or predictions of the other optical properties of the stratospheric aerosol, the spectral scattering phase function and the single-scattering albedo, along with the spectral variation of the optical depth, are available for the stratospheric aerosol, e.g., from inversions of $\tau_s(\lambda)$ measurements made at the surface to obtain the size distribution from which the other optical properties are computed.⁹ Only the stratospheric aerosol concentration was assumed to be unknown. It would be estimated based on the measurement of $\rho_t^{(s)}(1380)$. The reflectance at 1380 nm was then scaled, by the ratio of the single-scattered stratospheric aerosol reflectances at λ to that at 1380 nm, and subtracted from the reflectances in the visible and NIR, i.e.,

$$T(\lambda)\rho_t(\lambda) = \rho_t^{(s)}(\lambda) - \frac{\omega_s(\lambda)\tau_s(\lambda)p_s(\theta_v, \phi_v; \theta_0, \phi_0; \lambda)}{\omega_s(1380)\tau_s(1380)p_s(\theta_v, \phi_v; \theta_0, \phi_0; 1380)} \times \rho_t^{(s)}(1380),$$

where

$$p_s(\theta_v, \phi_v; \theta_0, \phi_0; \lambda) = P_s(\theta_-, \lambda) + [r(\theta_v) + r(\theta_0)]P_s(\theta_+, \lambda),$$

$$\cos \theta_{\pm} = \pm \cos \theta_0 \cos \theta_v$$

$$- \sin \theta_0 \sin \theta_v \cos(\phi_v - \phi_0),$$

and $r(\alpha)$ is the Fresnel reflectance of the interface for an incident angle α . Parameters $\tau_s(\lambda)$, $\omega_s(\lambda)$, and $P_s(\alpha, \lambda)$ are, respectively, the stratospheric aerosol optical thickness, single-scattering albedo, and scattering phase function for a scattering angle α . An-

gles θ_0 and ϕ_0 are, respectively, the zenith and azimuth angles of a vector from the point on the sea surface under examination (pixel) to the Sun, and likewise, θ_v and ϕ_v are the zenith and azimuth angles of a vector from the pixel to the sensor. These are measured with respect to the *upward* normal so θ_v and θ_0 are both less than 90° . At 1380 nm, $r(\alpha)$ was set to zero because the radiation at this wavelength cannot interact with the surface. The resulting values of $\rho_t(\lambda)$ were then inserted into the correction algorithm and the error at 443 nm was determined. This procedure is based on the assumption that the stratospheric aerosol enhancement of ρ_t is all due to single scattering.

5. As in procedure 4 it was assumed that all of the optical properties of the aerosol are known except the concentration. A one-layer multiple-scattering code (with a totally absorbing lower surface to represent the troposphere) was used to determine $\tau_s(1380)$ from $\rho_t^{(s)}(1380)$. This determines all of the optical properties of the stratospheric aerosol. These properties were inserted into a one-layer multiple-scattering code (with a Fresnel-reflecting sea surface as the lower boundary) to compute $\delta\rho_t^{(s)}(\lambda)$, which was subtracted from measured reflectances $\rho_t^{(s)}(\lambda)$ to provide $T(\lambda)\rho_t(\lambda)$. The resulting values of $\rho_t(\lambda)$ were then inserted into the correction algorithm and the error at 443 nm was determined. This procedure is similar to that in procedure 4; however, the single-scattering approximation was replaced by a full multiple-scattering computation. It is based on the assumption that there is *no radiative interaction* between the stratospheric aerosol layer and the other two layers in the visible.

6. Except for the step in which $\delta\rho_t^{(s)}(\lambda)$ is removed from $\rho_t(\lambda)$, this procedure is identical to procedure 5. Once all of the optical properties of the stratospheric aerosol are known, they were inserted into a *two-layer* multiple scattering code (as opposed to a *one-layer* code in procedure 5 above) with a Fresnel-reflecting sea surface as the lower boundary. The top layer consisted of the stratospheric aerosol and the lower layer had only Rayleigh scattering. This incorporated the Rayleigh-stratospheric aerosol interaction explicitly (albeit approximately because of the absence of the tropospheric aerosol), leaving only the Rayleigh-tropospheric aerosol and stratospheric-tropospheric aerosol interactions not addressed. After subtraction of the result of this computation from $\rho_t^{(s)}(\lambda)$, the result was inserted into the standard correction algorithm in which allowance was made for the fact that $\rho_r(\lambda)$ has already been removed along with the stratospheric component. This approach is possible because the optical properties of the Rayleigh scattering layer as well as the stratospheric aerosol layer are completely known.

These approaches clearly require increasing computational complexity and increasing amounts of knowledge concerning the optical properties of the stratospheric aerosol. Although knowledge of the stratospheric aerosol optical properties may be good

in certain instances, e.g., the El Chichón aerosol,⁹ in general this will not be available.

7. Results for the Simplified Procedures

The procedures listed in Section 6 were all designed to utilize $\rho_t^{(s)}$ at 1380 nm to remove the stratospheric contribution to ρ_t . With the exception of the first, they all require an estimate of transmittance factor T . Unfortunately, because of the nature of the approximations in passing from Eq. (1) to Eq. (2), there is no *a priori* way to determine the appropriate T in a multiple-scattering regime. Initially we assumed $T = 1$, which would be appropriate in the single-scattering regime.

An examination of results of the individual cases revealed the following for most of the correction procedures: (a) for a given stratospheric aerosol model, the largest values of $\Delta[t\rho_w(443)]$, the resulting error in $t\rho_w$ at 443 nm, occur at the scan edge with $\theta_0 = 60^\circ$, where one would expect the largest effect of multiple scattering; (b) for a given θ_0 , the error for viewing at the scan center is usually less than the error at the scan edge; (c) the correction errors are usually negative (too much radiance has been assigned to the atmosphere), with the aged volcanic ash aerosol more negative than the others, presumably because of its moderate absorption; and (d) the general patterns of the correction error as a function of θ_0 at the scan center and edge for a given model remain the same as τ_b and τ_s are varied, but patterns for different stratospheric models are not similar. As one might expect, the most complex methods of dealing with the stratospheric aerosol (procedures 5 and 6 in Section 6) usually yielded the best overall correction; however, as long as $\tau_s \leq 0.05$, most of the procedures produced acceptable results (except at the scan edge with $\theta_0 = 60^\circ$). In the case of large optical thicknesses for cirrus clouds, the error became excessive, with none of the procedures producing satisfactory results.

To try to improve the retrieval of $t\rho_w$, we decided to attempt to model T . In the first model we assumed that most of the radiance being scattered by the stratospheric layer is scattered through small angles (Fig. 1 shows that this is certainly true for cirrus clouds). This being the case, the contribution of the downward path through the stratosphere to T is just the *irradiance* (or flux) transmittance, which is identical to the diffuse transmittance $t(\theta_0)$. We then argued that the upward radiance distribution can be approximated as diffuse (albeit poorly); hence its traverse through the stratosphere is also described by the stratospheric diffuse transmittance. Thus, $T(\theta_0, \theta_v) \approx t(\theta_0)t(\theta_v)$. This assumption for T led to large positive errors in the water-leaving reflectance, which suggested that T was reduced too far from unity. However, the pattern of the error did suggest that a better result would be obtained with $T(\theta_0, \theta_v) \approx t(\theta_0)$. This in fact worked fairly well, and a sample of the results using this approximation for T are provided in Figs. 5 and 6 for $\tau_b = 0.15$. As in Figs. 3 and 4, in these figures we present histograms of the error

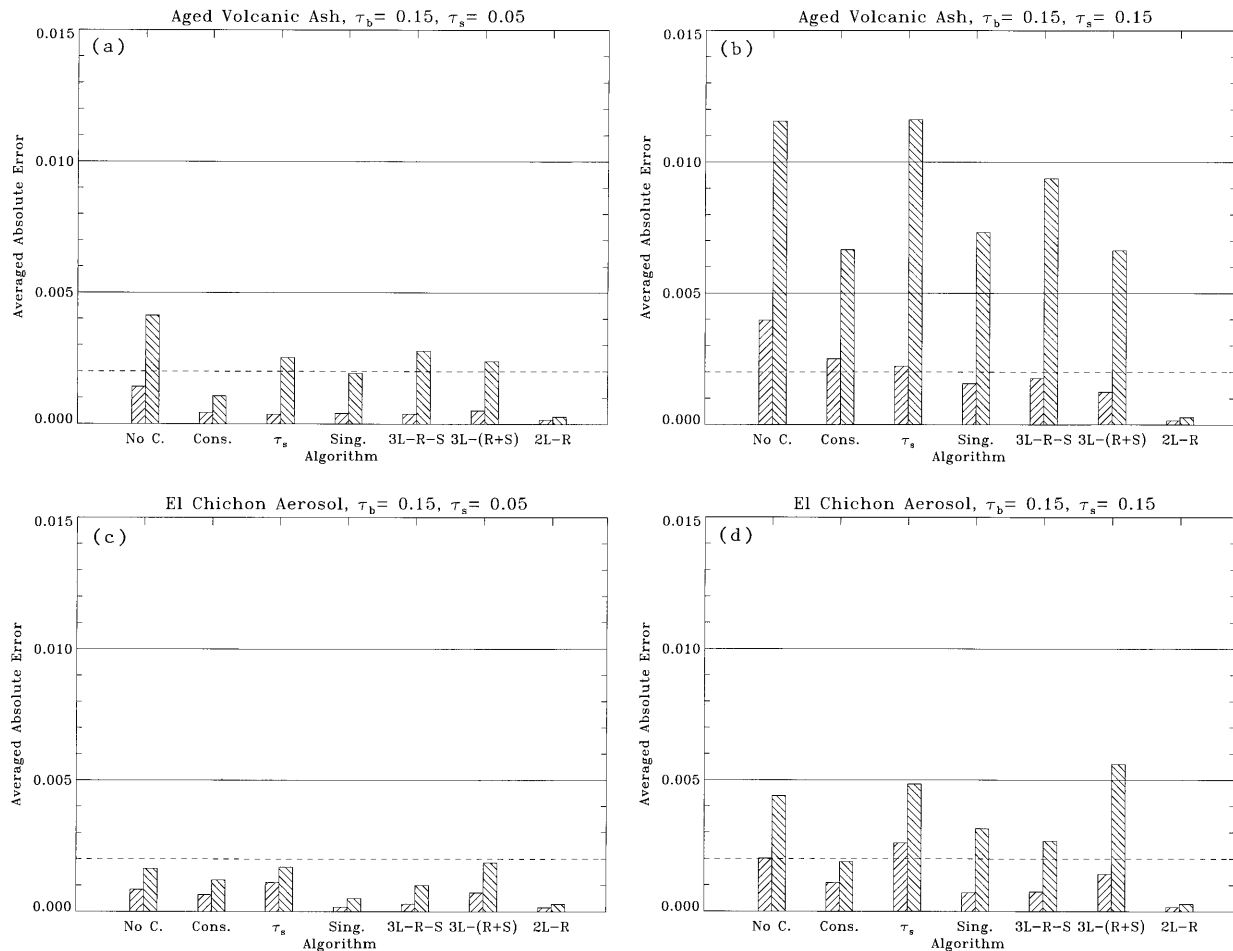


Fig. 5. Histogram of the average $|\Delta t_{p_w}(443)|$ (short bars) and the maximum $|\Delta t_{p_w}(443)|$ (tall bars) for the aged volcanic ash and the El Chichón stratospheric aerosols for $\tau_b(865) = 0.15$ and (a) $\tau_s(865) = 0.05$, (b) $\tau_s(865) = 0.15$, (c) $\tau_s(865) = 0.05$, (d) $\tau_s(865) = 0.15$.

as a function of the stratospheric aerosol removal procedure (procedures 1–6). Along the horizontal axes, No C. refers to procedure 1, Cons. refers to procedure 2, τ_s refers to procedure 3, Sing. refers to procedure 4, 3L-R-S refers to procedure 5, 3L-(R+S) refers to procedure 6, and 2L-R refers to the correction algorithm in the absence of stratospheric aerosol. The tall and short bars in Figs. 5 and 6 have the same meaning as those in Figs. 3 and 4. The results show that, with the exception of the scan edge at $\theta_0 = 60^\circ$, at least one of the procedures will usually produce a mean absolute error of <0.002 .

8. Semiempirical Approach for Correcting for Stratospheric Aerosols

The derivation of the results provided in Figs. 5 and 6 (except for procedure 1) required a model of the aerosol for the computation of diffuse transmittance T . Detailed stratospheric aerosol models are also required to provide $\delta\rho^{(s)}(\lambda)$ for the operation of procedures 4, 5, and 6. As models are already needed for these procedures, it is reasonable to use these models to estimate the *exact* value of T to use with each geometry and model. If the exact value of T does not depend too strongly on τ_b or on the aerosol properties

in the troposphere, then tables of T could be used to effect a better correction for stratospheric aerosols. As the required value of T will depend on the procedure used to correct for the stratosphere, one procedure must be selected. For this purpose, procedure 5 appears to be the best for three reasons. First, for cirrus clouds, which are expected to contaminate more of the imagery than volcanically produced stratospheric aerosol, procedure 5 reduces to the very simple procedure 2 because the optical properties are assumed to be independent of wavelength. Next, in contrast to procedure 6, procedure 5 requires no modification to the Gordon and Wang⁷ algorithm. Finally, procedure 2 assumes that the optical properties of the aerosol at λ are the same as at 1380 nm, which is only reasonable for cirrus clouds. Thus we use procedure 5 (which includes all significant orders of multiple scattering in the stratospheric layer) for the computation of T ; however, to make it reduce to procedure 2 for wavelength-independent aerosol, we modified the computation of the $\delta\rho^{(s)}$ so that there was no contribution from the sea surface at any wavelength, i.e., as a single layer above a totally absorbing surface. Figure 7 provides the resulting value of T

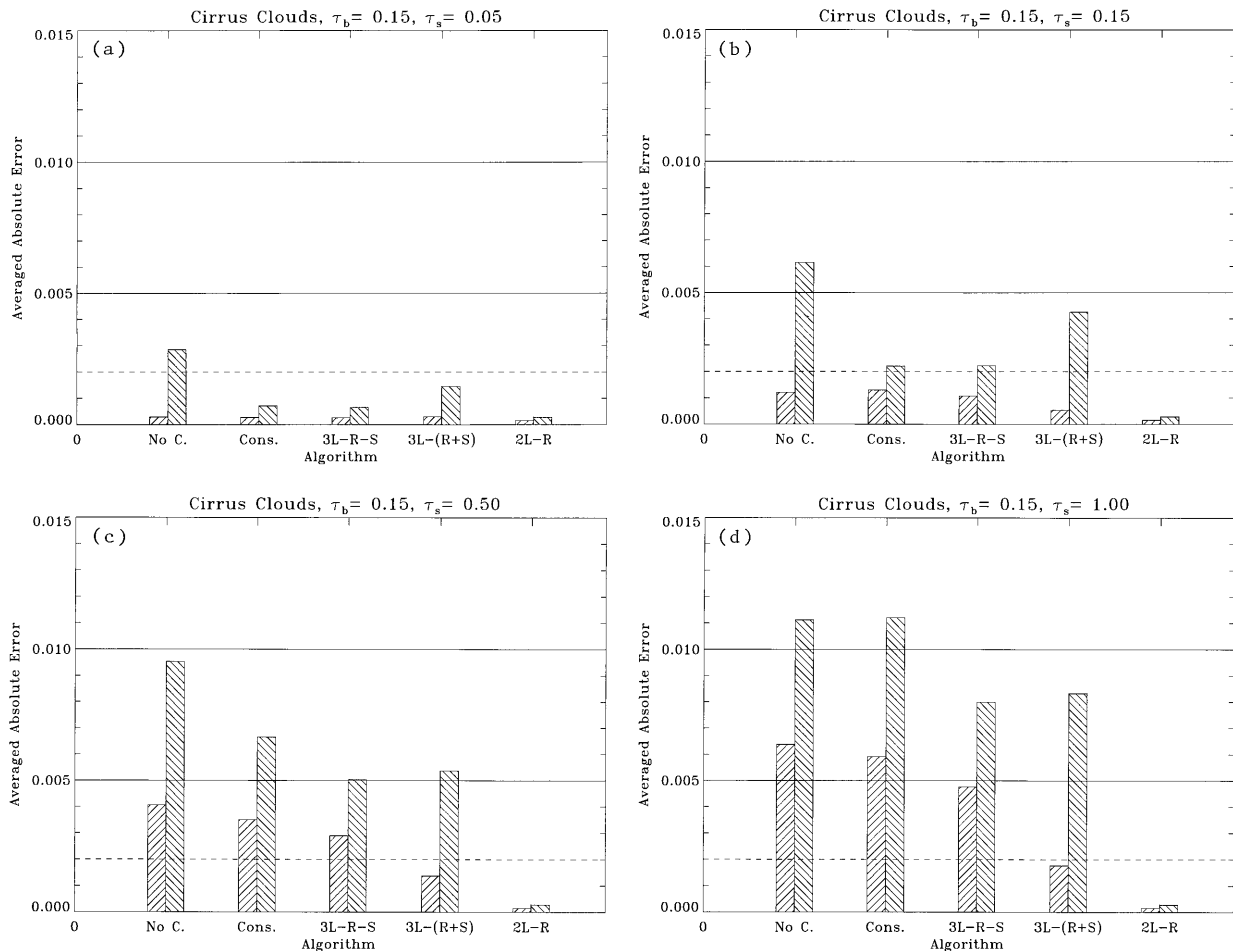


Fig. 6. Histogram of the average $|\Delta t_{\rho_w}(443)|$ (short bars) and the maximum $|\Delta t_{\rho_w}(443)|$ (tall bars) for the cirrus clouds with $\tau_b(865) = 0.15$: (a) $\tau_s(865) = 0.05$, (b) $\tau_s(865) = 0.15$, (c) $\tau_s(865) = 0.50$, (d) $\tau_s(865) = 1.00$.

as a function of the value of the reflectance at 1380 nm.

At 443 nm [Fig. 7(a)] it is seen that, for cirrus clouds, $T < 1$ and is remarkably insensitive to τ_b . In contrast, for 765 and 865 nm [Figs. 7(b) and 7(c)] $T > 1$ and is strongly dependent on τ_b . This indicates that in the NIR, multiple reflections between the stratosphere and the troposphere are very important. Multiple reflections must also be important in the visible, although their effects are apparently negated, possibly because of the strong limb brightening associated with multiple Rayleigh scattering compared with that of aerosols. Also, the insensitivity of T to variation in τ_b in the blue reflects the fact that most of S_{12}^- there is the result of Rayleigh scattering, not MBL aerosol. Similar effects are seen for the El Chichón and aged volcanic ash aerosols models. Clearly, the required values of T are strongly dependent on the stratospheric aerosol model.

The systematic variation of T with $\rho_t^{(s)}(1380)$ seen in Fig. 7 suggests that the measured value of $\rho_t^{(s)}(1380)$ could be used to estimate the proper value of T given the appropriate stratospheric aerosol model. We have tried to utilize this observation to make a better correction for stratospheric aerosols.

As we mentioned above, cirrus clouds are expected to contaminate more of the imagery than volcanically produced stratospheric aerosol; thus it is natural to employ the cirrus cloud model to estimate the value of T given $\rho_t^{(s)}(1380)$. To effect the correction, we used the cirrus cloud model to compute the required values of T , producing figures similar to Fig. 7 for each of the seven combinations of θ_0 and θ_v . For each geometry, T was then fit by least squares to a parabola in $\rho_t^{(s)}(1380)$ by pooling the results for $\tau_b = 0.15$ and 0.30 . If T were to fit $\rho_t^{(s)}(1380)$ exactly, then when the stratospheric aerosol actually is cirrus clouds and they are removed by using T determined from $\rho_t^{(s)}(1380)$, and the atmospheric correction algorithm is operated by using the retrieved ρ_t as the input reflectance, the resulting error in $t\rho_w$ would be that shown in Fig. 4 in the absence of stratospheric aerosol (MBL). However, it is clear from Fig. 7 that the fit cannot be exact, so there will be some residual error in $t\rho_w$. In Figure 8 we show the residual error in $t\rho_w$ when this procedure is applied to the cirrus cloud pseudodata as before. Clearly, the residual error is significantly smaller than that shown in Fig. 6 for the six simple procedures in Section 6, and corrections appear possible even for large τ_s . Figure 9 shows the

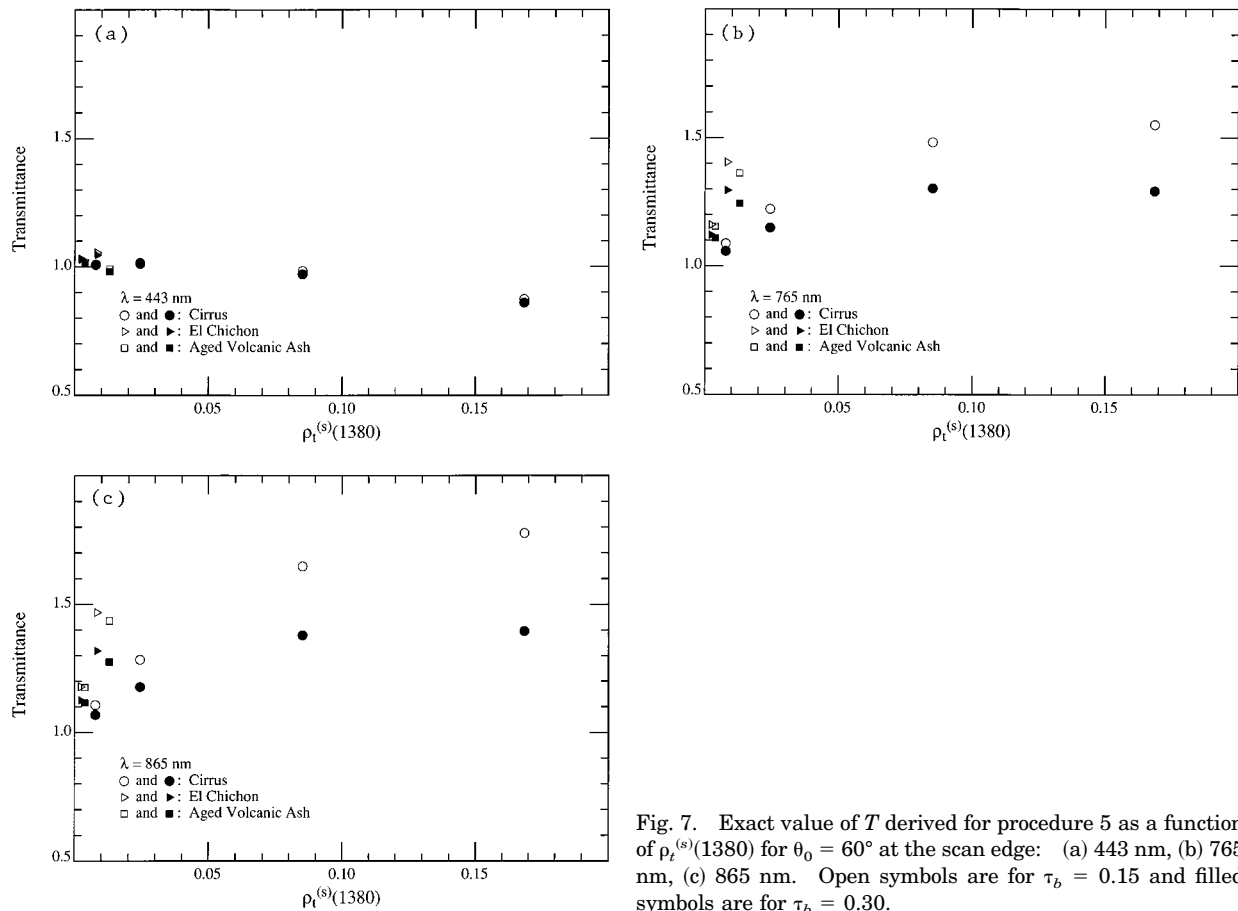


Fig. 7. Exact value of T derived for procedure 5 as a function of $\rho_t^{(s)}(1380)$ for $\theta_0 = 60^\circ$ at the scan edge: (a) 443 nm, (b) 765 nm, (c) 865 nm. Open symbols are for $\tau_b = 0.15$ and filled symbols are for $\tau_b = 0.30$.

residual error when this procedure is applied to pseudodata created with the El Chichón and aged volcanic ash aerosols in the stratosphere. Clearly, the results are poorer than those for cirrus clouds, and they are also poorer than those in Fig. 5 for the simplified procedures. Thus, it appears that if this method is to be used to correct for stratospheric aerosols, separate T versus $\rho_t^{(s)}(1380)$ relationships would

have to be used for volcanically derived stratospheric aerosols and for cirrus clouds.

In all of the simulations thus far, we have used the M80 aerosol model to represent the aerosol in the MBL. As the T versus $\rho_t^{(s)}(1380)$ relationship depends on τ_b (in the NIR), we expect that it might also depend on the aerosol type in the MBL. To study this dependence, we carried out a series of simula-

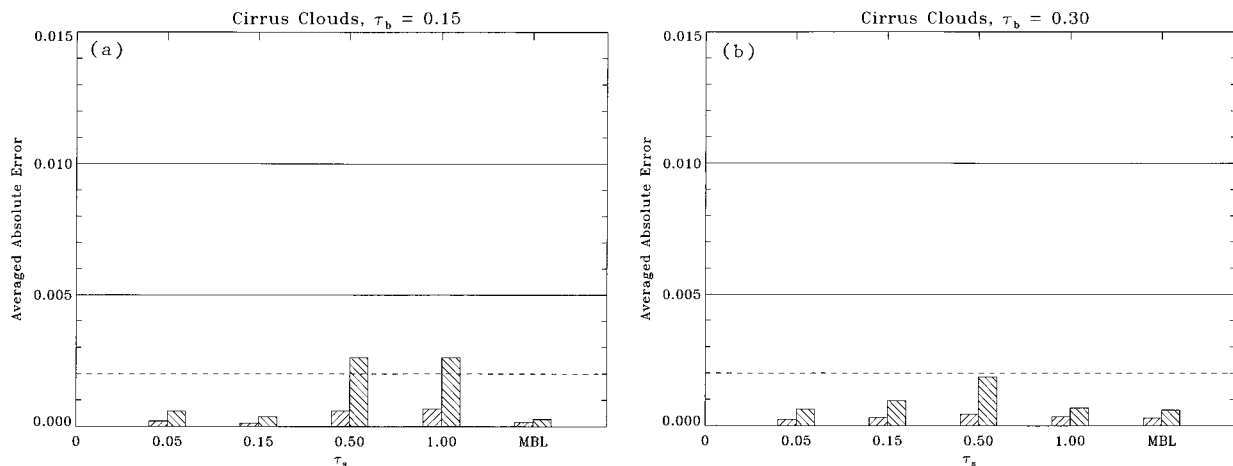


Fig. 8. Same as Fig. 4, except the stratospheric aerosol has been removed by using the T versus $\rho_t^{(s)}(1380)$ relationship derived for cirrus clouds in the stratosphere and M80 in the MBL as described in the text.

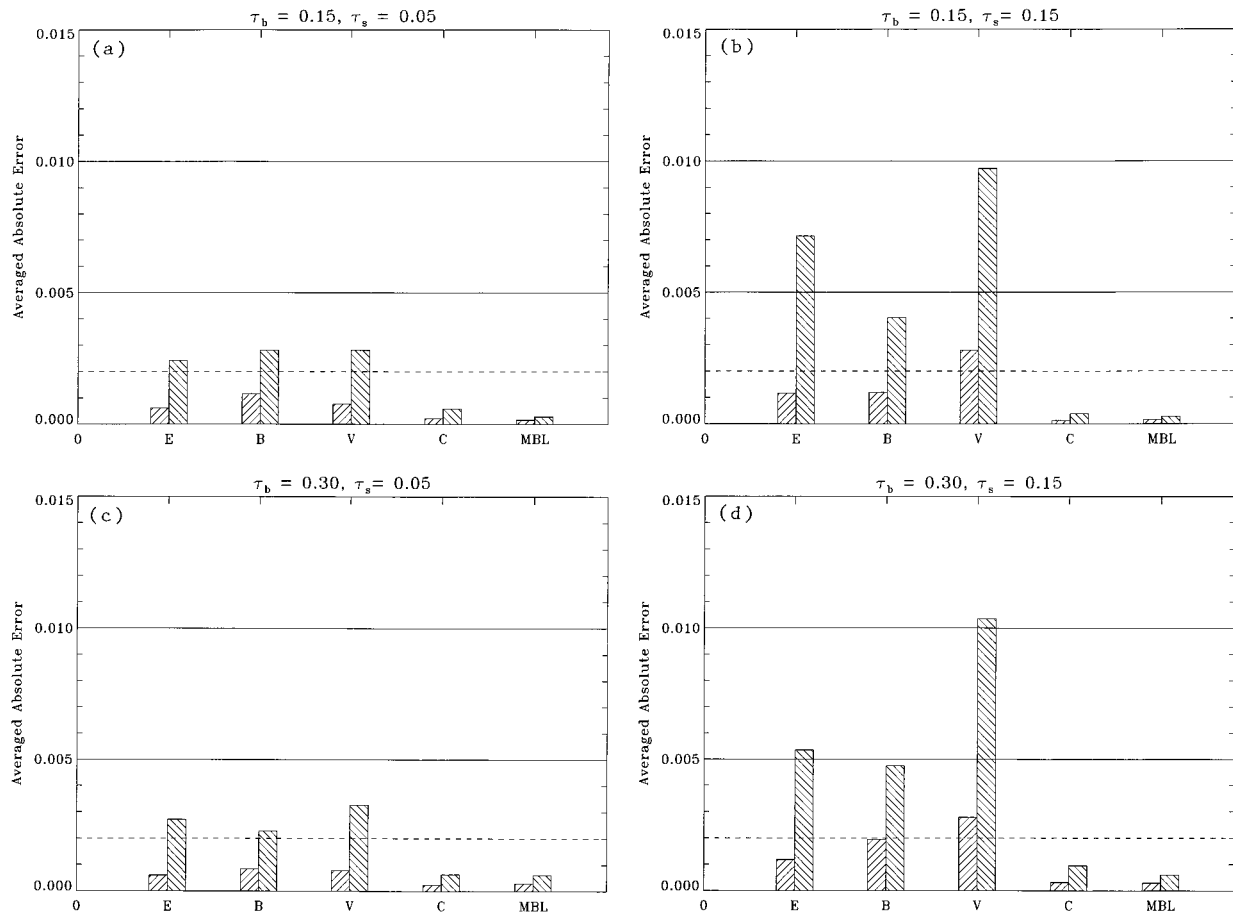


Fig. 9. Same as Fig. 3, except the stratospheric aerosol has been removed by using the T versus $\rho_t^{(s)}(1380)$ relationship derived for cirrus clouds in the stratosphere and M80 in the MBL as described in the text.

tions with the Shettle and Fenn¹⁵ tropospheric model at 80% relative humidity (RH) in the troposphere and cirrus clouds in the stratosphere. The scattering phase function for the tropospheric model at 80% RH (T80) shows much more scattering than M80 in the range of scattering angles from 40° to 140° , approximately the same amount for angles $>140^\circ$, and significantly less at small scattering angles (see Ref. 23, Fig. 4). Also, τ_b for T80 is a much stronger function of wavelength, with $\tau_b(443)/\tau_b(865) \approx 2.48$ compared with ≈ 1.16 for M80. This in itself makes atmospheric correction, even in the absence of stratospheric aerosols, more difficult for the T80 aerosol, given the same value of $\tau_b(865)$. The resulting T versus $\rho_t^{(s)}(1380)$ relationships are similar to those shown in Fig. 7; however, for a given value of $\rho_t^{(s)}(1380)$, the required value of T in the NIR is often considerably different from that for M80, although the general pattern is the same. Interestingly, at 443 nm there is very little difference in the required value of T between T80 and M80. This is in agreement with Fig. 7(a), which shows that T is nearly independent of τ_b in the blue. Clearly, if the T versus $\rho_t^{(s)}(1380)$ relationship generated for M80 is used when the actual aerosol in the MBL is T80, there will be a significant error in stratospheric aerosol correc-

tion in the NIR, and after application of the Gordon and Wang algorithm, error in the retrieved t_{ρ_w} . This is confirmed in Fig. 10, which provides results similar to those in Fig. 8, but for T80 in the MBL. Clearly, the results are not satisfactory, and they suggest that it is necessary to have some knowledge regarding the aerosol type in the MBL in order to improve on the correction.

We have examined the possibility of estimating the aerosol type in the MBL for the purpose of improving the correction, and it appears to be straightforward. Briefly, in the SeaWiFS atmospheric correction algorithm,⁷ in the absence of stratospheric aerosol, the spectral variation of $\rho_t - \rho_r$ between 765 and 865 nm is used to estimate a parameter called ϵ . This quantity is then compared with the value for individual members of a set of candidate aerosol models to determine a pair of models that best fit the variation. These models are then used to assess the multiple scattering and to extrapolate the aerosol contribution into the visible. We have found that when the T versus $\rho_t^{(s)}(1380)$ relationship derived from the M80 model is used to correct for stratospheric aerosols with either T80 or M80 located in the MBL, and the resulting values of ρ_t are inserted into the Gordon and Wang algorithm, the derived values of ϵ are very

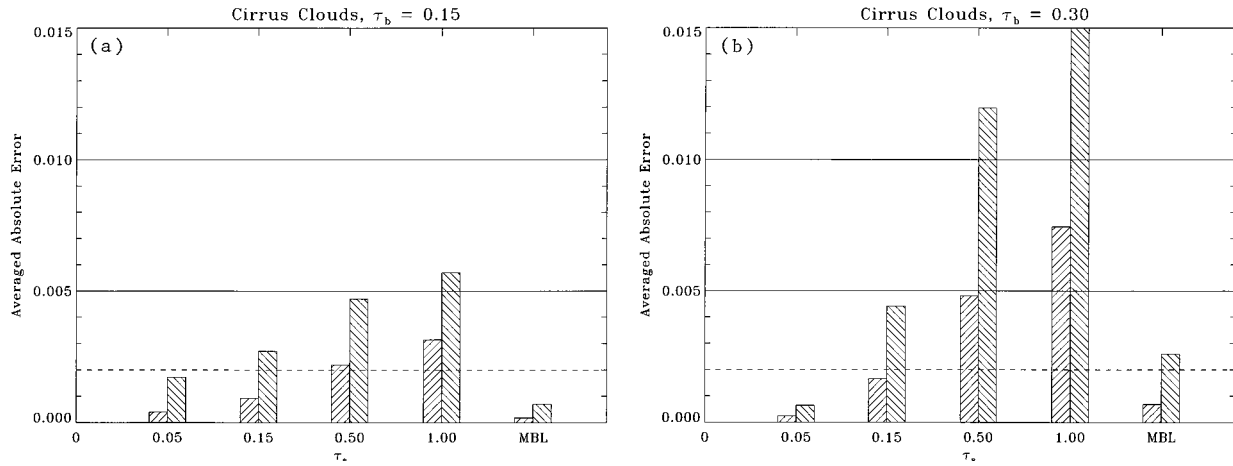


Fig. 10. Same as Fig. 8, except the aerosol described by T80 occupies the MBL, but the T versus $\rho_t^{(s)}(1380)$ relationship derived for cirrus clouds in the stratosphere and M80 in the MBL was used.

near the correct values, i.e., from the retrieved ϵ one would make a correct conclusion regarding which model (M80 or T80) is appropriate for the MBL. For example, in the geometry with the most multiple scattering, $\theta_0 = 60^\circ$ at the scan edge, with T80 in the MBL and $\tau_b = 0.15$, the combination cirrus cloud–MBL algorithms produced ϵ values of 1.185, 1.183, 1.180, 1.165, and 1.158 for $\tau_s = 0, 0.05, 0.15, 0.50$, and 1.00, respectively. These values should be compared with the true values of ϵ in the same geometry for the twelve candidate aerosol models in the Gordon and Wang algorithm. These are provided in Table 1. It is seen that for each value of τ_s , the combined algorithm chooses a candidate aerosol model between the tropospheric models at 70% and 90% relative humidity (RH)—exactly the position of T80—even though the T versus $\rho_t^{(s)}(1380)$ relationship was based on M80 in the MBL! This implies that it is feasible to estimate the aerosol type in the MBL even though an incorrect T versus $\rho_t^{(s)}(1380)$ relationship is used. Thus, we envisage a correction for thin cirrus clouds as follows. First the T versus $\rho_t^{(s)}(1380)$ relationship for M80 is used to estimate ρ_t . Next ρ_t is used in the Gordon and Wang algorithm to estimate ϵ . Finally, this value of ϵ is used to provide a more appropriate model for estimating the T versus $\rho_t^{(s)}(1380)$ relationship to be used to derive a final set of values for ρ_t . Thus there would be two passes through both the stratospheric correction algorithm and the Gordon and Wang algorithm, unless after the first pass it was decided that a second pass was not necessary, i.e., the retrieved ϵ was close to that for M80. If the aerosol model for the MBL is chosen judiciously, then much of the time only one pass through the combined algorithm would be necessary.

From our observations of the accuracy that ϵ could be estimated for T80 in the MBL by using the M80 T versus $\rho_t^{(s)}(1380)$ relationship, we prepared Fig. 11, which shows the overall error in atmospheric correction when the *correct* T80 T versus $\rho_t^{(s)}(1380)$ relationship (derived by pooling the $\tau_b = 0.15$ and 0.30 simulations) is used with T80 in the MBL. Clearly,

accurate corrections in the presence of cirrus clouds would be possible with such an algorithm. It should be noted that further improvement on this procedure is possible, as the first pass through the algorithm could be used to estimate τ_b as well as the aerosol type. Thus, a T versus $\rho_t^{(s)}(1380)$ relationship tailored to the MBL aerosol type and concentration could be utilized. This would provide significantly better results than those shown in Figs. 8 and 11.

Finally, the implementation of these ideas requires a model of the scattering properties of the aerosol. In contrast to volcanically produced stratospheric aerosol, in the case of cirrus clouds there is little likelihood that accurate estimates of the scattering phase function will be available *a priori*. Thus it is of interest to understand how inaccuracies in the cirrus cloud phase function will influence the T versus $\rho_t^{(s)}(1380)$ relationship, and ultimately the quality of the atmospheric correction. To effect this, we have examined an extreme case: we rederived the T versus $\rho_t^{(s)}(1380)$ relationship, with M80 in the MBL, by replacing the cirrus cloud phase function [Fig. 1(d)] with the phase function for *isotropic* scattering.

Table 1. Value of ϵ for the 12 Candidate MBL Models Used in the Gordon and Wang Correction Algorithm

Model	RH (%)	ϵ
Maritime	50	1.079
Maritime	70	1.066
Maritime	90	1.020
Maritime	99	0.983
Coastal	50	1.115
Coastal	70	1.101
Coastal	90	1.049
Coastal	99	1.008
Tropospheric	50	1.207
Tropospheric	70	1.198
Tropospheric	90	1.153
Tropospheric	99	1.112

^aParameter ϵ values are at the scan edge for $\theta_0 = 60^\circ$.

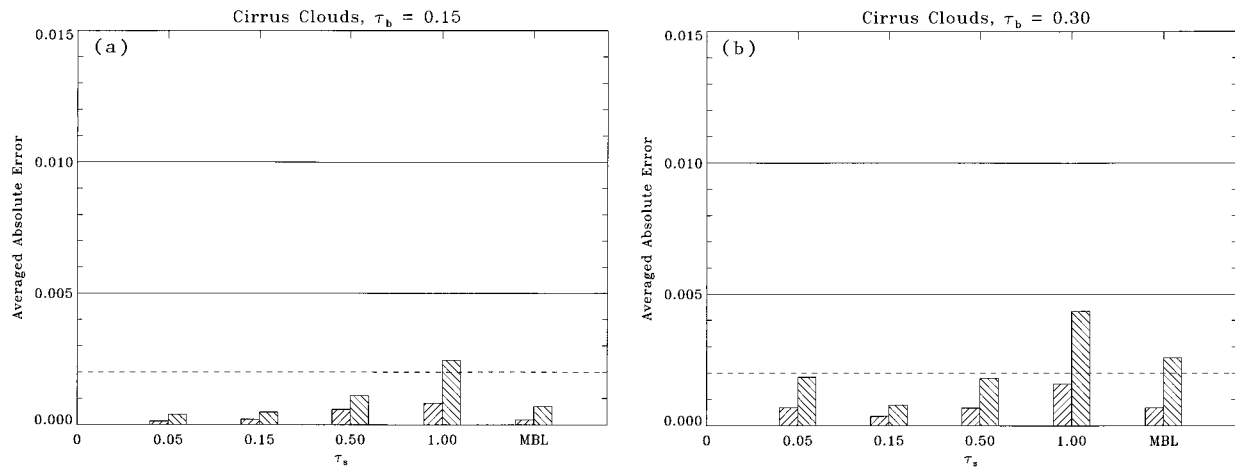


Fig. 11. Same as Fig. 10, except the T versus $\rho_t^{(s)}(1380)$ relationship derived for cirrus clouds in the stratosphere and T80 in the MBL was used.

As before, T was fit by least squares to a quadratic function of $\rho_t^{(s)}(1380)$ for each geometry by pooling the results for $\tau_b = 0.15$ and 0.30 . Figure 12 provides the atmospheric correction error resulting from the use of this relationship for cases with M80 in the MBL. Figure 12 should be compared to Fig. 8, in which the correct phase function was used to derive the T versus $\rho_t^{(s)}(1380)$ relationship, and to Fig. 4, in which no cirrus cloud correction was applied. Clearly, when the correct phase function is used (Fig. 8) the best results are obtained; however, the isotropic phase function produces acceptable corrections up to $\tau_s \approx 0.5$.

The fact that isotropic scattering provides a realistic T versus $\rho_t^{(s)}(1380)$ relationship is not surprising considering that, with the exception of the strong forward scattering and the halo peaks ($\sim 22^\circ$ and 46°), the cirrus cloud phase function [Fig. 1(d)] varies by less than an order of magnitude. Of course, a given $\rho_t^{(s)}(1380)$ is reached at a much lower value of τ_s when the isotropic phase function is used, because the strong forward peak in Fig. 1(d) (which makes a ma-

ior contribution to τ_s) is almost irrelevant in the T versus $\rho_t^{(s)}(1380)$ relationship. Thus, in reality, for a given τ_s , it is more accurate to say that the correct phase function has been replaced by the combination of a Dirac delta function in the forward direction and a scattering angle-independent constant elsewhere. These simulations suggest that a precise estimate of the phase function is not critical for cirrus clouds.

9. Discussion and Concluding Remarks

In this paper we have investigated the effect of the presence of stratospheric aerosol on the atmospheric correction of ocean color sensors. The goal of the study was twofold: (a) to estimate the severity of the degradation of atmospheric correction by using the Gordon and Wang⁷ algorithm, and (b) to examine several methods of removal of the stratospheric component by using the MODIS 1380-nm spectral band prior to application of the Gordon and Wang algorithm. This latter goal is of particular interest because, if it were possible to remove the stratospheric component, little or no modification of the present

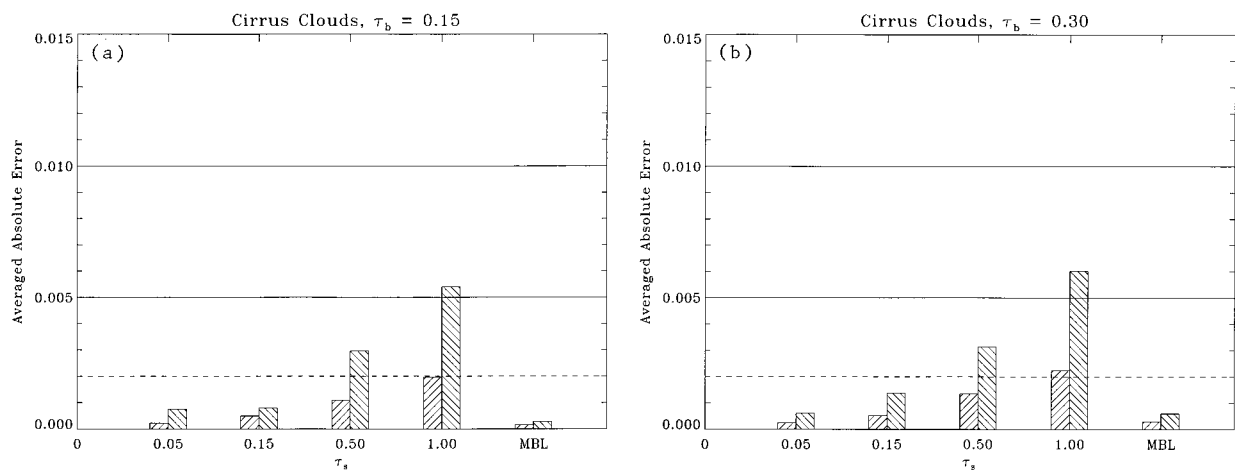


Fig. 12. Same as Fig. 8, except the T versus $\rho_t^{(s)}(1380)$ relationship was derived by assuming an isotropic scattering phase function for the cirrus clouds.

atmospheric correction algorithm would be required to accommodate correction for the stratospheric aerosol. After it was shown that a precise correction is not possible because of the lack of knowledge of the aerosol in the MBL, six simple procedures were examined for addressing the effect of the stratospheric aerosol, ranging from simply ignoring its presence (procedure 1) to requiring full knowledge of its spectral optical properties (procedures 4–6).

As one might expect, the stratospheric aerosol correction procedure requiring full knowledge of the spectral optical properties (except the concentration that would be determined by the reflectance at 1380 nm) and employing multiple and interactive scattering between stratospheric aerosol and tropospheric molecular scattering in the visible (procedure 6) usually yielded the best overall correction at large values of τ_s when combined with the Gordon and Wang algorithm. However, at small values of τ_s this was often not significantly better than the simplest procedure (2), and sometimes it was worse. The fact that procedure 1, simply ignoring the stratospheric aerosol, provides a reasonable correction for small τ_s agrees with the conclusion of Gordon and Castaño⁸ that the presence of the El Chichón aerosol had little effect on the CZCS atmospheric correction, taking into consideration that the CZCS did not require as accurate a correction as the MODIS.

Subsequently, we examined a semiempirical stratospheric aerosol correction scheme in which a generalized transmittance T was determined in such a manner as to provide the exact value of ρ_t for each geometry and combination of MBL and stratospheric aerosols. We found that this approach appears to be feasible for atmospheric correction, and we proposed an overall stratospheric–MBL correction algorithm. In the case of thin cirrus clouds, this algorithm should typically yield $t\rho_w$ with an error that is within the acceptable range for τ_s as large as 1.00. This is rather remarkable considering that the perturbation caused by the presence of the cirrus cloud was not small. For example, in the absence of the cirrus cloud for $\theta_0 = 60^\circ$ at the scan edge with $\tau_b = 0.15$, $\rho_t(\lambda) \approx 0.18, 0.036$, and 0.028 at 443, 765, and 865 nm, respectively, while $\rho_t^{(s)}(1380) \approx 0.0078, 0.024, 0.085$, and 0.17 for $\tau_s = 0.05, 0.15, 0.5$, and 1.0 , respectively. Thus, even at $\tau_s = 0.15$, the cirrus contribution alone is comparable with the value of the total reflectance at 865 nm in its absence.

Several simplifying assumptions were used in our simulations: (a) all of the tropospheric aerosol was assumed to be in the MBL; (b) all of the radiance exiting the top of the atmosphere at 1380 nm was assumed to be due to scattering from the stratospheric aerosol alone; (c) there was assumed to be no water vapor above the stratospheric aerosol, and (d) there was assumed to be no horizontal variability in the stratospheric aerosol optical thickness. Thus our simulations are an idealization, as in reality some radiance at 1380 nm can originate from below the stratospheric aerosol either from molecular scattering in the free troposphere or possibly even from the

MBL under conditions of very low relative humidity.²⁴ Also, there may be water vapor above thin cirrus clouds, in which case their reflectance would be underestimated at 1380 nm, and finally, cirrus clouds typically display considerable horizontal structure.

Other than the errors introduced through these simplifying assumptions, we see two remaining difficulties in applying this algorithm in practice: first, at low τ_s it is necessary to be able to determine whether the principal contributor to $\rho_t^{(s)}(1380)$ is thin cirrus or volcanically produced aerosol (Fig. 9); second, in order to utilize the algorithm to remove volcanically produced stratospheric aerosol, the full optical properties of the aerosol are required, with $\rho_t^{(s)}(1380)$ providing the concentration and T . It may be possible to distinguish thin cirrus from volcanically produced aerosol by an examination of the pixel-to-pixel variation in $\rho_t^{(s)}(1380)$, as the horizontal variability of cirrus should be much greater. Alternatively, it may be possible to distinguish them by using MODIS bands in the thermal IR. Correction for volcanically produced stratospheric aerosol following an eruption will be possible only after the optical properties of the aerosol are estimated and become stable.

From the computations presented here, we recommend that the semiempirical procedure be developed as an operational method of correcting for cirrus clouds, and to the extent that they can be separated from volcanically produced aerosol, for this as well. In addition to the large set of lookup tables required for operation of the Gordon and Wang⁷ algorithm, implementation of this algorithm would require a second set of lookup tables of the T versus $\rho_t^{(s)}(1380)$ for each, or at least some, MBL models for each stratospheric aerosol model.

The authors thank the National Aeronautics and Space Administration for support under grant NAGW-273 and contract NAS5-31363.

References

1. H. R. Gordon and A. Y. Morel, *Remote Assessment of Ocean Color for Interpretation of Satellite Visible Imagery: A Review* (Springer-Verlag, New York, 1983), p. 114.
2. W. A. Hovis, D. K. Clark, F. Anderson, R. W. Austin, W. H. Wilson, E. T. Baker, D. Ball, H. R. Gordon, J. L. Mueller, S. Y. E. Sayed, B. Strum, R. C. Wrigley, and C. S. Yentsch, "Nimbus 7 coastal zone color scanner: system description and initial imagery," *Science* **210**, 60–63 (1980).
3. H. R. Gordon, D. K. Clark, J. L. Mueller, and W. A. Hovis, "Phytoplankton pigments derived from the Nimbus-7 CZCS: initial comparisons with surface measurements," *Science* **210**, 63–66 (1980).
4. S. B. Hooker, W. E. Esaias, G. C. Feldman, W. W. Gregg, and C. R. McClain, *SeaWiFS Technical Report Series: Volume 1, An Overview of SeaWiFS and Ocean Color*, Tech. Mem. 104566 (NASA, Greenbelt, Md., July 1992).
5. V. V. Salomonson, W. L. Barnes, P. W. Maymon, H. E. Montgomery, and H. Ostrow, "MODIS: advanced facility instrument for studies of the Earth as a system," *IEEE Geosci. Remote Sensing* **27**, 145–152 (1989).
6. H. R. Gordon and D. K. Clark, "Atmospheric effects in the

- remote sensing of phytoplankton pigments," *Boundary-Layer Meteorol.* **18**, 299–313 (1980).
7. H. R. Gordon and M. Wang, "Retrieval of water-leaving radiance and aerosol optical thickness over the oceans with SeaWiFS: a preliminary algorithm," *Appl. Opt.* **33**, 443–452 (1994).
 8. H. R. Gordon and D. J. Castaño, "The Coastal Zone Color Scanner atmospheric correction algorithm: influence of El Chichón," *Appl. Opt.* **27**, 3319–3321 (1988).
 9. M. D. King, Harshvardhan, and A. Arking, "A Model of the Radiative Properties of the El Chichón Stratospheric Aerosol Layer," *J. Climate Appl. Meteorol.* **23**, 1121–1137 (1984).
 10. K. Ding and H. R. Gordon, "Analysis of the influence of O₂ A-band absorption on atmospheric correction of ocean color imagery," *Appl. Opt.* **34**, 2068–2080 (1995).
 11. B.-C. Gao, A. F. H. Goetz, and W. J. Wiscombe, "Cirrus cloud detection from airborne imaging spectrometer data using the 1.38 micron water vapor band," *Geophys. Res. Lett.* **20**, 301–304 (1993).
 12. P. Y. Deschamps, M. Herman, and D. Tanre, "Modeling of the atmospheric effects and its application to the remote sensing of ocean color," *Appl. Opt.* **22**, 3751–3758 (1983).
 13. H. R. Gordon, D. K. Clark, J. W. Brown, O. B. Brown, R. H. Evans, and W. W. Broenkow, "Phytoplankton pigment concentrations in the Middle Atlantic Bight: comparison between ship determinations and Coastal Zone Color Scanner estimates," *Appl. Opt.* **22**, 20–36 (1983).
 14. H. R. Gordon and M. Wang, "Influence of oceanic whitecaps on atmospheric correction of SeaWiFS," *Appl. Opt.* **33**, 7754–7763 (1994).
 15. E. P. Shettle and R. W. Fenn, "Models for the aerosols of the lower atmosphere and the effects of humidity variations on their optical properties," Tech. Rep. AFGL-TR-79-0214 (U.S. Air Force Geophysics Laboratory, Hanscomb Air Force Base, Mass., 1979).
 16. Y. Sasano and E. V. Browell, "Light scattering characteristics of various aerosol types derived from multiple wavelength lidar observations," *Appl. Opt.* **28**, 1670–1679 (1989).
 17. WCP-112, "A preliminary cloudless standard atmosphere for radiation computation," WMO/TD-No. 24 World Meteorological Organization, Geneva, 1986).
 18. K. F. Palmer and D. Williams, "Optical constants of sulfuric acid; application to the clouds of Venus?," *Appl. Opt.* **14**, 208–219 (1975).
 19. Y. Takano and K. N. Liou, "Solar radiative transfer in cirrus clouds. Part I: Single-scattering and optical properties of hexagonal ice crystals," *J. Atmos. Sci.* **46**, 224–240 (1989).
 20. H. C. van de Hulst, *Multiple Light Scattering* (Academic, New York, 1980), p. 739.
 21. P. J. Reddy, F. W. Kreiner, J. J. Deluisi, and Y. Kim, "Aerosol optical depths over the Atlantic derived from shipboard sun-photometer observations during the 1988 Global Change Expedition," *Global Biogeochem. Cycles* **4**, 225–240 (1990).
 22. G. N. Plass, G. W. Kattawar, and F. E. Catchings, "Matrix operator theory of radiative transfer 1: Rayleigh scattering," *Appl. Opt.* **12**, 314–328 (1973).
 23. M. Wang and H. R. Gordon, "Estimating aerosol optical properties over the oceans with the multiangle imaging spectroradiometer: some preliminary studies," *Appl. Opt.* **33**, 4042–4057 (1994).
 24. E. Ben-Dor, "A precaution regarding cirrus cloud detection from airborne imaging spectrometer data using the 1.38 μm water vapor band," *Remote Sensing Environ.* **50**, 346–350 (1994).